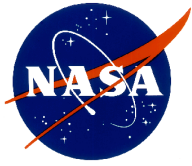JPL Document D-81562



# Exoplanet Exploration Program Technology Plan

# Appendix: 2013

P. R. Lawson

**National Aeronautics and Space Administration**

**Jet Propulsion Laboratory
California Institute of Technology
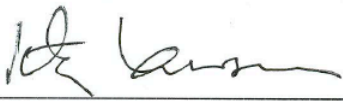Pasadena, California**

*21 January 2014*

# Approvals

**Released by**

_(signature)_               1/21/2014.

_____       _____

Peter Lawson, Exoplanet Exploration Program Chief Technologist, JPL

**Approved by**

_____       _____

Gary Blackwood, Exoplanet Exploration Program Manager, JPL

_____       _____

Douglas Hudgins, Exoplanet Exploration Program Scientist, NASA HQ

_____       _____

Anthony Carro, Exoplanet Exploration Program Executive, NASA HQ

# Contents

# Appendix A
# Exoplanet Technology Objectives

## A.1 Introduction

The purpose of this appendix is to guide near-term (1–5 year) technology development for future space observatories related to NASA's Exoplanet Exploration Program (ExEP). A long-term goal of the Program is a New Worlds mission, such as that envisaged by Astro2010: a mission capable of directly imaging terrestrial planets in the habitable zones of stars in the Solar neighborhood, and measuring their spectra to search for the telltale signs of life.  Such a mission will require some form of starlight suppression, and new technology developments will be needed to achieve the extreme degree of contrast that will be required.

Through this work it should also be possible in the near term to enable other missions whose science is compelling and essential to understanding the birth and evolution of planetary systems and the conditions that lead to life in the Universe.

The subjects covered here are only those most directly relevant to recommendations in the 2010 Decadal Survey of Astronomy and Astrophysics (Astro2010) [1], with regard to a *New Worlds Technology Development Program* and a future *New Worlds Mission*. The greatest emphasis is therefore placed on starlight-suppression technology to enable the detection of Earth-like planets around Sun-like stars.

The necessary technology developments and ongoing activities are summarized in this appendix.   An excellent overview of the challenges of direct imaging can be found in the volume *Exoplanets*, edited by S. Seager [2]. The interested reader will find additional details concerning exoplanet technology in the SPIE Conference Series on *Techniques and Instrumentation for the Detection of Exoplanets*, the most recent being Proc. SPIE vol. 8864.

## A.1.1   Program Goals

The 2010 Decadal Survey in Astronomy and Astrophysics  (NRC 2010) recommended the creation of a *New Worlds Technology Development Program* to advance the technological readiness of the three primary starlight suppression architectures: coronagraphs, starshades, and interferometers. The Survey further recommended—if the scientific groundwork and design requirements were sufficiently clear—that an architecture downselect should be made at the mid-decade, and a significantly increased technology investment over the latter half of the decade should be focused to prepare a mission concept based on this architecture for consideration by the 2020 Survey.

"Thus the plan for the coming decade is to perform the necessary target reconnaissance surveys to inform next-generation missions while simultaneously completing the technology development to bring the goals within reach." (NWNH, p. 39)

In response to the survey recommendations, the NASA *Astrophysics Implementation Plan* describes a path leading to the selection of the next strategic mission after the James Webb Space Telescope. While emphasizing the priority of the Wide-Field Infrared Survey Telescope (WFIRST), the plan includes studies for exoplanet probe-scale missions as possible alternatives.

In support of this effort an implementation of WFIRST is being studied that uses a 2.4-m telescope of the Astrophysics Focused Telescope Assets (AFTA) that were donated to NASA, and an exoplanet coronagraph is being studied as a second instrument for this mission. AFTA coronagraph technology is the subject of a separate technology plan being developed by the AFTA Study Office to be published in early 2014. The outline of that plan is described here to illustrate how its development will also advance other coronagraph efforts, primarily through advances in common technologies and augmentations to the Program's testbed infrastructure. The technology described in this document, however, is devoted to probe-scale missions and future (non-AFTA) NWNH missions.

NASA's Exoplanet Exploration Program supports activities that contribute to the advancement of these exoplanet mission concepts. The Program funds and facilitates experiments and analyses selected by NASA HQ through yearly solicitations issued through the NASA omnibus Research Opportunities in Space and Earth Sciences (ROSES). The Program also provides support in the form of infrastructure, expertise, and test facilities that have been developed in prior years.

As a part of ROSES, NASA currently funds technology development through the Astrophysics Research and Analysis (APRA) solicitation and the Technology Development for Exoplanet Missions (TDEM) component of the Strategic Astrophysics Technology (SAT) solicitation. APRA covers low-TRL technology research while SAT-TDEM covers maturation of mid-range TRL technologies. This two-stage approach supports the advancement of technology envisaged by Astro2010. TDEM tasks funded for the 2009, 2010, and 2012 solicitations are listed in Tables A.1 and A.2.

The goal of exoplanet technology development is to enable future missions by demonstrating selected key technologies. This effort must include the establishment of performance error budgets tied to flight requirements and experimental demonstrations that the error budgets, or key components of the error budgets, can be met. Furthermore, models must be validated that demonstrate that the physics of the limiting error sources in those experiments are understood well enough to reliably predict the performance of the flight mission.

The recommendation by the Decadal Survey was to continue to pursue the development of coronagraph, external occulter, and interferometer technologies to allow an architecture downselect by the late-Decade. Nevertheless, for both cost and technical readiness reasons, infrared interferometry is currently of lower priority as the basis for a *New Worlds Mission* than either of the coronagraph or starshade architectures.

## A.1.2   Coronagraph and Starshade STDT

The NASA *Astrophysics Implementation Plan* includes studies for exoplanet probe-scale missions as possible alternatives. In 2013–2014 the teams involved in these efforts are

developing detailed observatory and mission designs, as well as an independent list of technology gaps and priorities. The interested reader is encouraged to consult the reports generated by these teams when they become publicaly available.

## A.1.3   Previously Funded Efforts

Tables A.1 and A.2 list the previously funded TDEM awards, grouped by research area. The results of these efforts are described in the text in Sections A.3 and A.4.

Table 1. Starlight Suppression Technology research funded through the Technology Development for Exoplanet Missions component of NASA's solicitation on Strategic Astrophysics Technology. Awards for calls from 2009, 2010, and 2012 are listed. Each award nominally provides two years of funding. The 2009 awards were funded in 2010 and continued through 2012. The 2010 awards were funded in 2012 and so should continue through 2014. These efforts are described in further detail in Section A.4 and A.5.

| Year | PI | Institution | Proposal Title |
|------|-----|-------------|----------------|
| CORONAGRAPH STARLIGHT-SUPPRESSION DEMONSTRATIONS | | | |
| 2009 | John Trauger | JPL/Caltech | Advanced Hybrid Lyot Coronagraph Technology for Exoplanet Missions |
| 2010 | Eugene Serabyn | JPL/Caltech | Demonstrations of Deep Starlight Rejection with a Vortex Coronagraph |
| 2009 | Olivier Guyon | Univ. of Arizona | Phase-Induced Amplitude Apodization Coronagraphy Development and Laboratory Validation |
| 2010 | Olivier Guyon | Univ. of Arizona | Advances in Pupil Remapping (PIAA) coronagraphy: improving Bandwidth, Throughput and Inner Working Angle |
| 2009 | Mark Clampin | NASA/GSFC | Visible Nulling Coronagraph Technology Maturation: High Contrast Imaging and Characterization of Exoplanets |
| 2010 | Richard Lyon | NASA/GSFC | Compact Achromatic Visible Nulling Coronagraph Technology Maturation |
| 2010 | Jagmit Sandhu | JPL/Caltech | Visible Nulling Coronagraph (VNC) Technology Demonstration Program |
| STARSHADE TECHNOLOGY | | | |
| 2009 | N. Jeremy Kasdin | Princeton University | Starshades for Exoplanet Imaging and Characterization: Key Technology Development |
| 2010 | N. Jeremy Kasdin | Princeton University | Verifying Deployment Tolerances of an External Occulter for Starlight Suppression |
| 2012 | Suzanne Casement | Northrop Grumman Aerospace Systems | Starshade Stray Light Mitigation through Edge Scatter Modeling and Sharp-Edge Materials Development |
| 2012 | Tiffany Glassman | Northrop Grumman Aerospace Systems | Demonstration of Starshade Starlight-Suppression Performance in the Field |

Table A.2 Supporting Technologies research funded through the Technology Development for Exoplanet Missions component of NASA's solicitation on Strategic Astrophysics Technology. Awards for calls from 2009 and 2010 are listed. These efforts are described in further detail in Section A.4 and A.7.

| Year | PI | Institution | Proposal Title |
|------|-----|-------------|----------------|
| WAVEFRONT SENSING & CONTROL OF SCATTERED STARLIGHT | | | |
| **2009** | Martin Noecker | Ball Aerospace | Advanced Speckle Sensing for Internal Coronagraphs and Methods of Isolating Exoplanets from Speckles |
| **2010** | N. Jeremy Kasdin | Princeton University | Integrated Coronagraph Design and Wavefront Control using Two Deformable Mirrors |
| **2010** | Paul Bierden | Boston Micromachines Corporation | MEMS Deformable Mirror Technology Development for Space-Based Exoplanet Detection |
| **2010** | Michael Helmbrecht | Iris AO | Environmental Testing of MEMS Deformable Mirrors for Exoplanet Detection |
| CORONAGRAPH MODELING AND MODEL VALIDATION | | | |
| **2009** | John Krist | JPL/Caltech | Assessing the Performance Limits of Internal Coronagraphs Through End-to-End Modeling |
| **2010** | Stuart Shaklan | JPL/Caltech | Coronagraph Starlight Suppression Model Validation: Coronagraph Milestone #3A |
| DETECTOR TECHNOLOGY* | | | |
| **2009** | Donald Figer | Rochester Inst. Tech. | A Photon-Counting Detector for Exoplanet Missions |

\* Topic area excluded from the TDEM element of SAT in subsequent ROSES calls.

## A.1.4   Exclusions and Constraints for ROSES 2013

TDEM is primarily directed at supporting technologies for the development of exoplanet coronagraphs and starshades, with an emphasis on enabling specific future missions. In the context of efforts in this decade, the missions under consideration are probe-scale coronagraph, probe-scale starshade missions, and the AFTA-WFIRST coronagraph. As explained below, the AFTA coronagraph is being developed with directed funding and so proposals related to its development are not being solicited in the 2013 TDEM call. 2013 TDEM proposals should therefore address the technology needs of other identifiable mission concepts and not be duplicative of efforts being undertaken for AFTA.

Considering the limited available resources, exclusions are listed in the TDEM solicitation to help guide proposers. These exclusions are listed below for reference. Should there be any questions concerning the exclusions, the governing document is the current online version of the solicitation available at NSPIRES.

### *Technologies with Goals other than the direct detection of exoplanets*

Investigations that advance technologies for future missions with goals other than the direct detection of extrasolar planets (e.g. astrometry, high-precision photometry, transit spectroscopy) are not solicited at this time.

### Technologies for direct detection of exoplanets with Infrared Interferometry

The recommendation by the Decadal Survey was to continue to pursue the development of coronagraph, external occulter, and interferometer technologies to allow an architecture downselect by the late-Decade. Nevertheless, for both cost and technical readiness reasons, infrared interferometry is currently of lower priority as the basis for a future mission than either of the coronagraph or starshade architectures. Technologies leading to the development of infrared interferometry are not solicited.

### Selected Supporting Technologies

Technologies that are specifically excluded from the SAT/TDEM solicitation at this time include are (1) detector technology, (2) mirror technology (with the exception of adaptive systems associated with wavefront sensing and control in coronagraphs), (3) telescope assembly technology, (4) spacecraft sunshields and thermal control, (5) propulsion systems, (6) vibration isolation systems, (7) spacecraft pointing control, and (8) formation flying technology (with the exception of formation flying sensors and algorithms in support of external occulter mission concepts).

### System-level Performance Demonstration and Modeling of AFTA-like Obstructed Aperture Coronagraphs

Coronagraph technologies specific to the AFTA aperture, being advanced through the AFTA-WFIRST technology development effort, are not eligible for funding through the SAT solicitation. Technologies that are not eligible include: (1) Masks/apodizers for Shaped-pupil, Hybrid Lyot, and Phase-Induced Amplitude Apodization Complex Mask (PIAA-CMC) coronagraphs; (2) Low-order wavefront sensing and control; (3) Data post-processing; (4) System-level performance demonstration and modeling of AFTA *obscured* aperture systems.

### Limited access to ExEP High-Contrast Imaging Testbeds

Proposers interested in coronagraph technologies, other than those supporting an AFTA coronagraph, should be aware that the advancement of an AFTA coronagraph will nearly fully subscribe the time available on the ExEP High Contrast Imaging Testbeds. There will be very limited time available to support new coronagraph TDEM demonstrations that require these testbeds.

### Predictive and Post-Test Modeling

All SAT/TDEM investigations that propose high-contrast imaging demonstrations are now required to perform both predictive and post-test validated modeling as part of their effort. In the interests of consistency and comparability, investigators will be expected to make use of the ExEP's existing modeling capability.

### Suborbital Programs

Due to budgetary constraints, proposals for suborbital programs are not solicited at this time.

# A.2 AFTA & Coronagraph System Technology

The following subsections are included here to highlight areas of planned AFTA technology development that would also be supportive of other coronagraph concepts. Because these technologies will be developed through directed funding, SAT-TDEM proposals are not solicited in these areas.

The main technology challenges of the AFTA coronagraph are due to the fact that its telescope was never designed for coronagraphy. It uses an input pupil that is obscured by a large secondary mirror, which in turn is supported by six struts. This introduces complex diffraction features that are absent in designs that use unobscured pupils. Consequently, the masks and selected input optics will require technology development that is specific to AFTA. Nonetheless, demonstrations of AFTA technology will require augmentations and improvements to other technologies and testbed infrastructure that may be made available to test other concepts. A non-exhaustive list of technologies to be developed by AFTA is described here. Technology development for the AFTA coronagraph will be the subject of a separate technology plan to be published by the AFTA Study Office early in 2014.

## A.2.1 Low-order Wavefront Sensing & Control

A slight misalignment of the coronagraph would cause starlight to appear at the edge of the dark hole of the coronagraph and could mimic the presence of a planet. It is therefore important to validate the design of a suitable pointing control system for a coronagraph. This would integrate the control of the coronagraph's fine-steering mirror with the control of the body pointing of the spacecraft.

A first step in this direction was accomplished with the development of the Phase-Induced Amplitude Apodization coronagraph system in the HCIT-2 testbed. Sub-milliarcsecond pointing stability was demonstrated in vacuum with a servo system, with the intent of eventually expanding it to demonstrate low-order wavefront sensing and control [26].

A low-order wavefront sensor uses the bright starlight that is rejected by the coronagraph and measures not only pointing changes but low-order aberrations such as defocus, coma, and spherical aberration. Static and dynamic low-order wavefront errors are anticipated due to slight imperfections in the optical design and thermally induced mechanical distortions of the optics that might be experienced in flight. The corrections of low-order wavefront errors—other than pointing—has not yet been demonstrated and is a priorty of the AFTA technology development program.

High-order wavefront sensing, on the other hand, is accomplished by modulating the input wavefronts with reflection off one or more deformable mirrors and measuring phase changes in speckles at the science camera. However the sensing is accomplished in the dark hole, using the relatively few photons collected there by the coronagraph, and operates over much longer timescales. High-order wavefront sensing and control is routinely accomplished in the lab and is not currently an area of concern.

## A.2.2 Coronagraph System-level Performance Demonstration

To date all of the highest-contrast coronagraph demonstrations have been undertaken in the lab in a static vacuum environment, subject only to slow ambient changes in the

temperature of the lab. These demonstrations have been limited to contrast measurements only, without the presence of a simulated planet source.

In order to demonstrate coronagraph performance in a flight-like environment, the expected on-orbit disturbances to pointing and low-order wavefront errors must be simulated and compensated for using the necessary servo systems, as described above. Moreover, the planet detection demonstrations should be tailored to the inner working angle, spectral bandwidth, and raw contrast floor that are required in flight.

The input disturbances for AFTA will be simulated using an input tip-tilt stage and one or more deformable mirrors.

## A.2.3   Ultra-low Noise Visible Detectors

The AFTA coronagraph will need high-performance low-light level detectors for use in its science camera and its integral field spectrograph. Advances are needed in the achievable noise performance and in particular the quantum efficiency achievable in the wavelength range of 0.9–1.0 μm. There are several options, notably as the Electron-Multiplying CCDs manufactured by e2v. What follows is a description of related work funded through TDEM in prior years.

Donald Figer (Rochester Institute of Technology) was funded through a 2009 SAT-TDEM award to raise the technology readiness of Avalanche Photodiode (APD) arrays. A formal Milestone Whitepaper was approved by the Program for this effort [74]. The Milestone was phrased as follows:

Demonstrate the performance of a photon-counting 256×256 Geiger-Mode Avalanche Photodiode (GM-APD) focal plane array after radiation exposure. The array is designed to provide zero read-noise, ultra-high dynamic range, and highly linear response. The following characteristics are to be measured: dark current, intra-pixel response, total quantum efficiency, after-pulsing, persistent charge, and crosstalk. The measurements will be made before and after 50 krad (Si) ~60 MeV proton irradiation. Important performance parameters include read noise, dark counts, and total quantum efficiency. This work is being conducted through the Rochester Institute of Technology.

This effort is a demonstration of new detector technology that may greatly improve the science throughput of coronagraph and starshade mission concepts. This work is ongoing: a silicon 256×256 diode array has been bonded to a Read Out Integrated Circuit (ROIC); the array has been hybridized and tested [75]; and a first-light image has been obtained. This device has a 100% fill factor and a good response from 300–1000 nm. Radiation tests have been completed, but at the time of writing a final report has not yet been submitted. Future work in this area may include the performance validation of silicon focal plane arrays with a larger number of pixels (1024×1024 vs 256×256).

## A.2.4   PMN Deformable Mirror Technology

Wavefront aberrations less than 1/10,000th of a wave must be maintained in a coronagraph if contrasts of $1 \times 10^{-10}$ contrast are to be achieved. At visible wavelengths, this implies wavefront control at the level of 0.5 Å, and deformable mirror (DM) technology is therefore required to compensate for residual optical aberrations.

Two DMs are required to create a symmetric dark hole around the image of a star, correcting both amplitude and phase errors across the full available field of view. The

standard practice in lab experiments up until 2013 has been to use only a single DM and create a half dark-hole, offset to one side of the star.

The AFTA coronagraph will use 48 × 48 element PMN deformable mirrors made by AOA Xinetics. These mirrors represent the state of the art and are routinely used in the HCIT vacuum testbeds. They have produced all the reported results of contrasts better than $1 \times 10^{-9}$. The Xinetics PMN-based DMs have also been successfully vibration tested at JPL.

The DMs for the AFTA coronagraph will be implemented in the testbeds in a flight-like configuration: there will be a pair of DMs in the beampath prior to the starlight suppression optics, controlled to create a dark hole that is symmetric about the star.

Jeremy Kasdin (Princeton University) and collaborators were funded through a 2010 TDEM award to demonstrate 2-DM wavefront control using a Shaped Pupil Coronagraph. Their goal was to achieve better than $1 \times 10^{-9}$ raw contrast at 10% bandwidth. Raw contrasts of $3.6 \times 10^{-9}$ were achieved using an optical configuration that was not optimized for the demonstrations (due to scheduling constraints). A final report on these tests is pending.

# A.3 Coronagraph Technology Requirements

## A.3.1 Specialized Coronagraph Optics

A continuing program to advance the performance of masks, apodizers, or beam-shaping optics specific to non-AFTA coronagraphs is yet needed. This should include improved designs to minimize coronagraph chromaticity, improved fabrication methods to minimize defects or discretization effects in masks, and the development and testing of circularly-symmetric masks. Demonstrated results in this area are summarized by Lawson et al. (2013) and are described below and illustrated in Figs. A.1 and A.2.

There are several approaches to the design of coronagraph instruments. Such instruments may include implementations of intensity masks [4], phase masks [6], phase-induced amplitude apodization [7], shaped pupils [8], visible nulling coronagraphs [9], or hybrid designs [10].

The state of the art demonstrated in the lab is summarized in Fig. A.1. Most notable amongst these results is a contrast of $2 \times 10^{-10}$ with a 2% bandwidth and $2 \times 10^{-9}$ with a 20% bandwidth at 3–15$\lambda$/D achieved through the use of 4th order band-limited Lyot hybrid masks [11]. Models exist that match these results, although they have not yet been formally validated. Other results plotted in Fig. A.1 are described in the follow subsections.

### Hybrid Lyot Masks

The Hybrid Lyot masks are image-plane masks that appear as a linear fringe pattern of metal deposited on glass, with an additional (thus hybrid) layer of dielectric to compensate for residual phase errors.

One deformable mirror (DM) is used in the experiments, whereas two would be used in flight. The masks that have been used have all been linear masks, because the manufacturing process is simpler. Circularly symmetric masks would no doubt be manufactured for a flight mission. Although the designs of circular masks exist, none have yet been fabricated. The current limitation in performance is understood to be the ability to accurately deposit the required thickness of dielectric.

The throughput can be estimated from the effective pupil shear used in the mask design, which for the results reported here was a shear of 36% of the pupil thus yielding a throughput of 56% past the Lyot stop. Polarizers are not used.

John Trauger (JPL/Caltech) with a 2009 TDEM award demonstrated mean raw contrasts of $3.2 \times 10^{-10}$ with a 10% bandwidth in a 284 ($\lambda$/D)$^2$ field extending from 3–16 $\lambda$/D. Raw contrasts of $1.3 \times 10^{-10}$ were demonstrated with a 20% bandwidth.

### Phase-Induced Amplitude Apodization

Phase-Induced Amplitude Apodization (PIAA) uses pairs of aspheric mirrors to reshape the pupil-plane intensity distribution, providing a Gaussian-like (prolate spheroidal) distribution and eliminating diffraction sidelobes. Results have been reported from two separate facilities. In-air experiments are reported from the NASA Ames Coronagraph Experiment (ACE) by Belikov et al., and from the vacuum High Contrast Imaging Testbed (HCIT) at the Jet Propulsion Laboratory.

Table A.3 Coronagraph Technology Gaps Listed in Priority Order.

| ID | Title | Description | Current | Required |
|---|---|---|---|---|
| **C-1** | Specialized Coronagraph Optics | Masks, apodizers, or beam-shaping optics to provide improved planet detection capability. | A linear mask design has yielded $3.2\times10^{-10}$ mean raw contrast from 3–16 $\lambda$/D with 10% bandwidth using an unobscured pupil in a static lab demonstration. | Circularly symmetric masks with a larger discovery space and IWA ≤ 3$\lambda$/D with contrasts ≤ $1\times10^{-9}$ for NWNH. |
| **C-2\*** | Low-order Wavefront Sensing & Control | Slowly varying large-scale optical aberrations may mimic the signature of an exoplanet. | Tip/tilt errors have been sensed and corrected in vacuum with a stability of 0.001 $\lambda$/D at sub-Hertz frequencies. | Tip/tilt, focus, astigmatism, and coma sensed and corrected simultaneously to maintain raw contrasts of ≤ $1\times10^{-9}$ for NWNH. |
| **C-3\*** | Coronagraph System-level Performance Demonstration | High-fidelity laboratory contrast demonstrations that include simulated science targets and flight-like perturbations. | Star-only (no planet) contrast demonstrations in vacuum with an unobscured pupil and semi-static wavefront errors. | Testing in a flight-like dynamic environment with star, planet, and optical telescope assembly simulator with the telescope-specific pupil obscuration. |
| **C-4\*** | Ultra-low Noise Detector | Low-noise detectors for exoplanet characterization with an Integral Field Spectrograph. | Read noise of < 1 e$^-$/pixel has been demonstrated with EMCCDs in a 1k × 1k format. | Read noise < 0.1e$^-$/pixel in a ≥ 2k × 2k format in a flight-like radiation environment. |
| **C-5** | Deformable mirrors | Maturation of deformable mirror technology toward flight readiness. | Xinetics DMs and MEMS DMs have undergone partial environmental testing (see text). | Development of flight-like electronics. Full environmental system testing with post-test performance validation. |
| **C-6\*** | Post-processing of Data | Techniques are needed to characterize exoplanet spectra from residual speckle noise for typical targets. | Planets with contrasts between $10^{-5}$ and $10^{-6}$ have been detected in the near infrared. | Techniques must enable exoplanet characterization of of exoplanets with contrasts ≤ $10^{-10}$ for NWNH. |

*Topic being addressed by directed-technology development for the AFTA coronagraph.  To avoid redundancy, coronagraph technologies that will be substantially advanced under the AFTA-WIFRST technology development are not eligible for under the auspices of the SAT Program.

For the flight configuration, there would be two DMs located before the input PIAA optics and there would be a second (inverse) set of PIAA optics after the focal-plane mask and prior to the science camera. With this arrangement the outer working angle is limited by the number of actuators on the DM, as is the case with other coronagraphs. However, for the laboratory demonstrations there is only one DM located between the input PIAA optics and focal-plane mask and no inverse PIAA optics. Having the DM located *after* the PIAA optics is a convenience that simplifies the wavefront control, because the mapping of the DM elements is not altered by the PIAA optics. The angular extent of the dark holes that are demonstrated in the lab are limited by the number of actuators on the DM *and* the mapping of the PIAA. The mirror pairs used in the HCIT were not optimized for operations at broad-bandwidths, and new mirrors would be manufactured for flight. Polarizers were used in these experiments to improve the measured contrast.
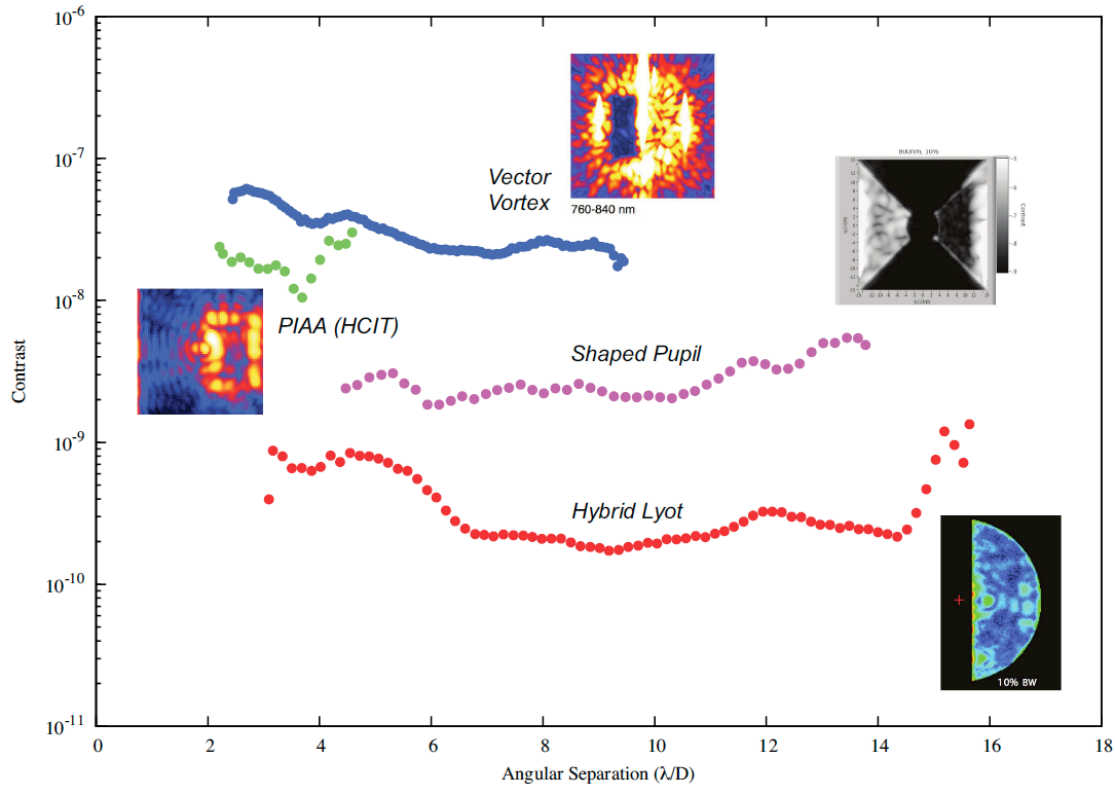


Fig. A.1: Coronagraph laboratory demonstrations using 10% bandwidth light.

The challenge of implementing PIAA optics lies in the design and manufacturing of these aspheres.

The PIAA optics would ideally have a throughput of 100%, however pupil and image-plane stops reduce the effective throughput to 92%. Because polarizers were used in these experiments, the actual throughput was approximately 46%.

Olivier Guyon (Univ. Arizona) with 2009 & 2010 TDEM awards demonstrated mean raw contrasts of $1.8 \times 10^{-8}$ with a 10% bandwidth in a field of 10 $(\lambda/D)^2$ extending from 2.2–4.6 $\lambda/D$. Raw contrasts of $1.3 \times 10^{-10}$ were demonstrated with in monochromatic light.

### Shaped Pupil Masks

The Shaped Pupil Coronagraph (SPC) is a binary pupil-plane mask that blocks or passes light in different regions of the pupil and thus shapes the point-spread function of the coronagraph in the image plane, digging out one or more dark holes.

These results made use of a linear Ripple-3 SPC with one deformable mirror and a layout closely similar to that of the Hybrid Lyot and Vector Vortex coronagraphs. It is likely that for a flight mission a new design would be created to take advantage of possible 2D optimization of the mask.

Two deformable mirrors would be used in flight. The challenge of manufacturing shaped pupil masks lies in the ability to machine features as small as 10-15 μm wide and thinned to a thickness of 50 μm or less. Narrower features are approximated by hole patterns.

The Ripple 3 mask has a geometric throughput of approximately 30%. The Airy throughput, which also accounts for light scattered in the wings of the point spread function, reduces the overall throughput to 10%. No polarizers were used in these experiments.

Ruslan Belikov (NASA ARC) as a graduate student at Princeton University in 2007 demonstrated mean raw contrasts of $2.5 \times 10^{-9}$ with a 10% bandwidth in a field 81 $(\lambda/D)^2$ extending from 4.5–14 $\lambda/D$. Raw contrasts of $1.2 \times 10^{-9}$ were demonstrated in 2% bandwidth light.

### Vector Vortex Masks

The Vector Vortex is an image-plane mask that adjusts the phase of the incoming field, producing a rotational phase ramp of two or more even number of cycles to cancel the on-axis starlight. For the results shown here, a liquid-crystal polymer vector vortex was used.

The optical configuration is essentially identical to that of the Hybrid Lyot architecture, having only one DM for current testing, but likely using two for flight. No fundamental change to the mask design would be needed for flight. The current limitation in performance is related to the ability to manufacture masks with a vortex pattern that is maintained to very small offsets from the center of rotation, and to extend the designs to broadband multi-layer masks. For the current experiments, a polarizer is required prior to the pinhole of the source.

The throughput would ideally be 100%, but the Lyot stop was undersized to 85% for the monochromatic demonstrations and to 92% for the broadband demonstrations, yielding a 72% and 85% transmission respectively. Additionally a polarizer is used at the source (as mentioned above), and so the effective throughput is approximately 36% monochromatic and 43% broadband.

Eugene Serabyn (JPL/Caltech) with a 2010 TDEM award demonstrated mean raw contrasts of $3.2 \times 10^{-8}$ with a 10% bandwidth in a 60 $(\lambda/D)^2$ field extending from 2.4–9.4 $\lambda/D$. Raw contrasts of $4.3 \times 10^{-9}$ were demonstrated in monochromatic light.
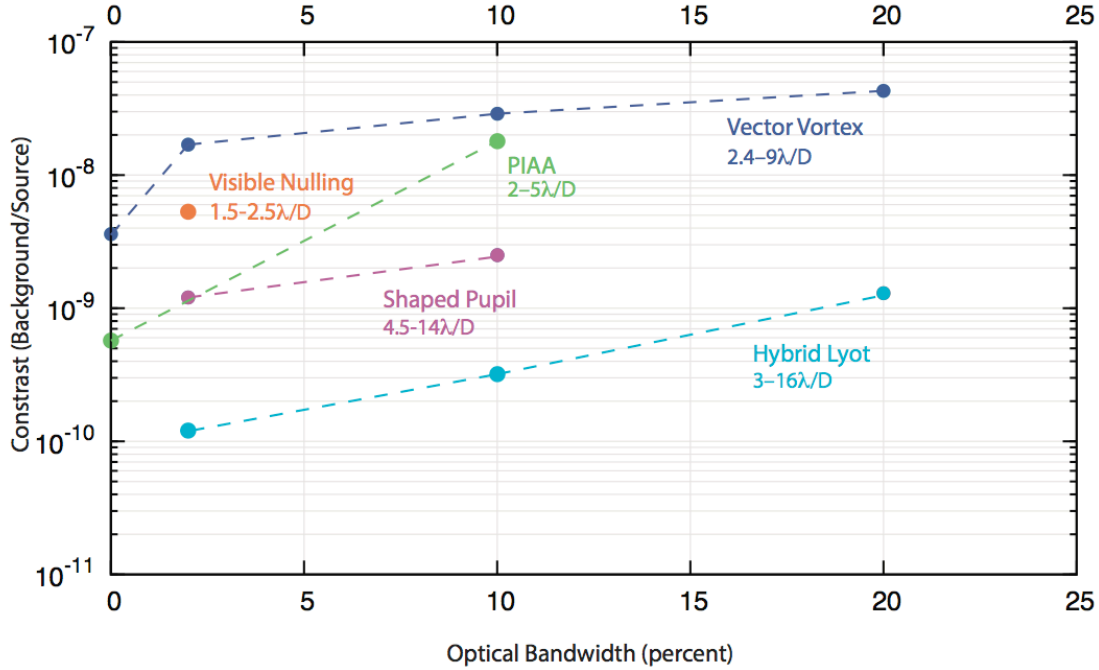
Fig. A.2: Demonstrated coronagraph contrast as a function of bandwidth. This plot summarizes results described in the text. Results reported by PIs or found in the published literature are denoted by the filled circles. Milestone results are denoted by the filled squares. The mean contrast is plotted for results that are averaged over a dark hole, ie. averaged over an area of 4–10 $\lambda$/D in the case of the metallic band-limited mask. The Earth/Sun contrast at visible wavelengths would be approximately $10^{-10}$.

### Visible Nulling Coronagraphs

A Visible Nulling Coronagraph (VNC) uses an interferometer back-end to reject starlight via interferometric nulling with a sheared pupil. This approach uses a deformable mirror, typically in combination with an array of single-mode optical fibers.

In a flight configuration, two VNC combiners would be used in series (one for each of two orthogonal image axes), whereas the results reported here use only a single VNC combiner.

For flight a large outer working angle would be achieved using a deformable mirror with at least 925 segments. The lab demonstrations used a 169 segment deformable mirror and produced a wedge-shaped dark hole in the region of 2–5 $\lambda$/D. The flight combiners will use arrays of single-mode fibers, with the same number of fibers and the same geometrical arrangement as the segments in the DM, to provide spatial filtering and intensity balancing of light from each segment. These arrays were not used for the demonstrations reported here.

The VNC uses a shear of 25% of the pupil, which yields a geometric throughput of 69%. A linear polarizer was used for these experiments and so the effective throughput was approximately 35%. A new approach is anticipated for use in flight to allow both polarizations to be measured simultaneously.

Mark Clampin and Rick Lyon (NASA GSFC) with 2009 & 2010 TDEM awards demonstrated mean raw contrasts of $5.3 \times 10^{-9}$ with a 2% bandwidth in a 1.0 ($\lambda$/D)$^2$ field extending from 1.5–2.5 $\lambda$/D.

## A.3.2   MEMS Deformable Mirror Technology

Deformable mirror development is needed in two specific areas: 1) Miniaturization of drive electronics using low-power Application-Specific Integrate Circuits (ASICs) suitable for flight.  2) A continuing program of work with DMs in 64x64 format, including operational testing of existing devices and investigation of development paths for smaller pitch and improved surface quality.

There are no plans to advance MEMS DMs through AFTA.  However, through SAT-TDEM two separate 2010 awards were funded, to Iris AO and Boston Micromachines Corp., to continue environmental testing of both continuous face-sheet DMs as well as segmented MEMS DMs.

The goal of this effort is to better characterizing their failure modes, and thus raise the TRL of the respective DM models.  Work to date has focused on establishing the testing protocols upon which the success criteria of the Whitepapers will be based.  Paul Bierden is leading the effort on behalf of Boston Micromachines Corp.  Michael Helmbrecht is leading the effort on behalf of Iris AO.

Boston Micromachines MEMS DMs have undergone environmental testing [52] and have flown on a sounding rocket experiment [53], although in the latter case no performance data was acquired.  MEMS DMs have demonstrated a monochromatic raw contrast of $5.3 \times 10^{-9}$ over angular separations of 1.5–2.5 $\lambda$/D using a Visible Nulling Coronagraph.

## A.3.3   Other Coronagraph Technologies

### *Efficient Coronagraph Optical Modeling*

New efficient implementations of coronagraph modeling for the Vector Vortex Coronagraph (VVC), the Phase-Induced Amplitude Apodization (PIAA) coronagraph, and the Hybrid Band-Limited Coronagraph (HBLC) have been shown to be accurate to 1% or better relative to the mean field contrast for contrasts down to $10^{-10}$ [45] [46]. This represents a related activity because it does not include experimental validation of the models, as required in Coronagraph Milestone 3A. Models developed through this work were used to predict coronagraph performance with realistic wavefront errors [48].

This work was the subject of a 2009 TDEM award to John Krist (JPL/Caltech) and collaborators.  The effort was successfully completed and two technology milestone reports were approved by the Program [45] [48].  The source code for modeling this effort is now available at http://exep.jpl.nasa.gov/technology/.

### *Model Validation of Band-limited Coronagraphs*

To date no model of coronagraph performance has yet been experimentally validated, in the formal sense defined by TPF-C Milestone 3A. In 2011 initial work commenced to validate sensitivity models of band-limited coronagraphs using the same metallic mask used for TPF-C Milestone 2 [43].   Further progress was reported in 2012 [44].

The effort is being continued, led by Stuart Shaklan (JPL/Caltech) and funded through a 2010 SAT-TDEM award.  The TPF-C Milestone 3A Whitepaper, provides the foundation for this work [15].

### *Self-Coherent Sensing*

Coronagraphs may require integration times that are many hours long, not only to detect planets but also to sense wavefront errors. Coherent speckle detection methods may provide the means to more rapidly sense and correct wavefront errors. An approach similar to the Self-Coherent Camera [49] has been demonstrated in the HCIT using a pupil-plane mask with selectable pinholes. The goal was to demonstrate the capability to measure speckles of about $1 \times 10^{-8}$ contrast with uncertainty, stability, and repeatability of 20% in intensity and 1 radian in phase with 90% statistical confidence, in a window at least $2 \times 2$ $\lambda/D$ wide at $< 10\lambda/D$ from the star, in one spectral band of width $\geq 10\%$, with a uniform incoherent background of at least $1 \times 10^{-8}$ in the area covered by the point-spread function [50]. This represents a related activity that may improve the stability of starlight-suppression experiments.

This work was conducted by Stuart Shaklan for Steven Kendrick (Ball Aerospace and Technology Corporation) and collaborators, funded through a 2009 TDEM award and successfully completed in 2012 [51].

# A.4 Starshade Technology Requirements

External occulters, or starshades, block starlight by shadowing the entrance pupil of a telescope, using a physical separation between starshade and telescope sufficient to provide the necessary inner working angle. This typically requires the starshade to be tens of meters in diameter and located tens of thousands of kilometers from the telescope [54].

A starshade may have numerous petals that are each tapered to produce a desired apodization function, as seen from the telescope. The petal shapes also eliminate most edges that would otherwise diffract starlight toward the center of the image—thus suppressing the Poisson spot that would be present if a circular occulter were used. Independent optical modeling predictions have shown excellent agreement concerning the contrast sensitivity to petal shape errors [55], and detailed preliminary error budgets have been proposed [56].

Table A.4 Starshade Technology Gaps Listed in Priority Order.

| ID | Title | Description | Current | Required |
|---|---|---|---|---|
| **S-1** | Control of Scattered Sunlight | Sunlight scattered from starshade edges and surfaces risk being the dominant source of measurement noise. | Several preliminary designs of edge shapes have been studied through laboratory tests having edge radius $\geq 10\ \mu m$. | Edges manufactured of high flexural strength material with edge radius $\leq 1\ \mu m$. |
| **S-2** | Validation of starshade optical models | Experimentally validate the equations that predict the contrasts achievable with a starshade. | Experiments have validated optical diffraction models at Fresnel number of ~100 to contrasts of $4 \times 10^{-10}$, but with poor agreement near petal valleys and tips. | Experimentally validate models of starlight suppression to $\leq 1 \times 10^{-11}$, and perturbation intensities to 20% at Fresnel number of 10–20. |
| **S-3** | Starshade Deployment | Demonstrate that a starshade can be deployed to within the budgeted tolerances. | Millimeter-wave mesh antennas have been deployed in space with diameters up to 17m × 19m and a out-of-plane accuracy of 2.4-mm. | Demonstrate using a half-scale or larger prototype the budgeted in-plane deployment tolerances, which are millimeter to sub-millimeter depending on the specific error terms. |
| **S-4** | Petal Prototype Demonstration | Demonstrate a high-fidelity prototype starshade petal. | Low-fidelity petals have been assembled and precision petal manufacturing has been demonstrated. | Demonstrate a fully integrated petal, including blankets, edges, and deployment control interfaces. |
| **S-5** | Formation Flying GN&C | Demonstrate that the GN&C system for an occulter will enable the required slew from star to star and positional stability for science observations. | Simulations have shown that sensing and GN&C is tractable, though sensing demonstrations of lateral control has not yet been performed. | Sensors demonstrated with errors $\leq 0.25$ m. Control algorithms demonstrated with lateral control errors $\leq 1$m. |

Two similar approaches to the design of external occulters have been studied, differing by whether an analytical petal shape is used [57][58] or whether it derives from a mathematical optimization [59][60]. Several different implementations are being investigated for the packaging and deployment of a starshade: one example is the use of deployable booms [61][62]; another is the use an unfurling truss [63][64].

The subject areas for starshade milestones are described in the sections below and summarized in Table A.4. Preliminary Milestone topics are related to the materials, design, fabrication, and predicted optical performance of the as-built components and subsystems. Later milestones cover topics that must be demonstrated at the system level and include deployment, dynamic behavior, as well as guidance, navigation, and control. The final topic is analogous to the final pre-formulation milestone for coronagraphs: a demonstration that the on-orbit performance is achievable based upon a well-grounded understanding of the error budget, backed by the necessary laboratory results.

## A.4.1   Control of Scattered Sunlight

Sunlight scattered from an occulter may potentially overwhelm light from astrophysical sources in the field of view and risks being the dominant source of measurement noise. Of particular concern is wide-angle scattering of sunlight from the edges of starshade petals. Initial progress in this area has been reported by Martin (JPL/Caltech) and collaborators [72].

A milestone in the control of scattered light would be to demonstrate with a baseline external occulter design that the brightness of sunlight scattered from the occulter would be less than the brightness of exozodiacal light. This may include demonstrations of the control of light scattered from petal edges, transmitted through the occulter fabric, or reflected from other identified sources such as the Earth or Moon.

Research in this area will be conducted by S. Casement (Northrop Grumman) through a 2012 SAT-TDEM award with work to begin in early 2014.

## A.4.2   Validation of Starshade Optical Models

Laboratory and field experiments have substantially validated the theoretical models of starshade performance. These demonstrations have included the following: (1) Monochromatic tests done at Princeton University; (2) 50% bandwidth tests done through a 42.8-m vacuum chamber at Northrop Grumman Aerospace Technologies (NGAS); and (3) 50% bandwidth tests conducted by NGAS on the desert floor in Death Valley National Park. These experiments are illustrated in Fig. A.3.

The NGAS demonstrations use occulters with a flight-like profile, either suspended by supporting wires for tests in the lab or by a single strut for tests in the desert. The experiments from Princeton use an inverse occulter that could not be implemented in flight.

At Princeton University, the theoretical diffraction integral commonly used for occulter design has been optically validated for contrasts to $4.5 \times 10^{-10}$ [66]. At Northrop Grumman Aerospace Systems (NGAS) starlight suppression experiments using scaled starshades have produced rotationally-averaged contrasts of $2.6 \times 10^{-7}$ at the starshade mask's inner working angle—where the optical throughput drops to 50% [68]. Beyond the inner working angle yet within the apodized field-of-view, features as faint as $5 \times 10^{-10}$ have also been detected through experiments both at Princeton University and at the University of

Colorado. These experiments are designed to measure the starshade's shadow at the same Fresnel number as would be used in an actual flight-system, although not with the same inner working angle. The masks are centimeters in diameter and placed at about ten or tens of meters from the detector. Research is ongoing at Princeton University in 2012-2013.

The throughput of the occulter is 100% for objects lying at angular positions beyond the tips of the starshade.

Although the predicted starlight suppression has been demonstrated, forward scattering from the petal tips and valleys yet produces bright features that are not well modeled and are likely the result of extremely small edge errors in those regions. It is anticipated that those bright features will be largely suppressed through the use of physically larger test articles, as the manufacturing tolerances of the valley and tips will be reduced.

Tiffany Glassman (NGAS) has been funded through a 2012 TDEM to further pursue starshade optical testing using a multi-kilometer test range. Preliminary results using a 60-cm starshade have been reported in the literature [73].
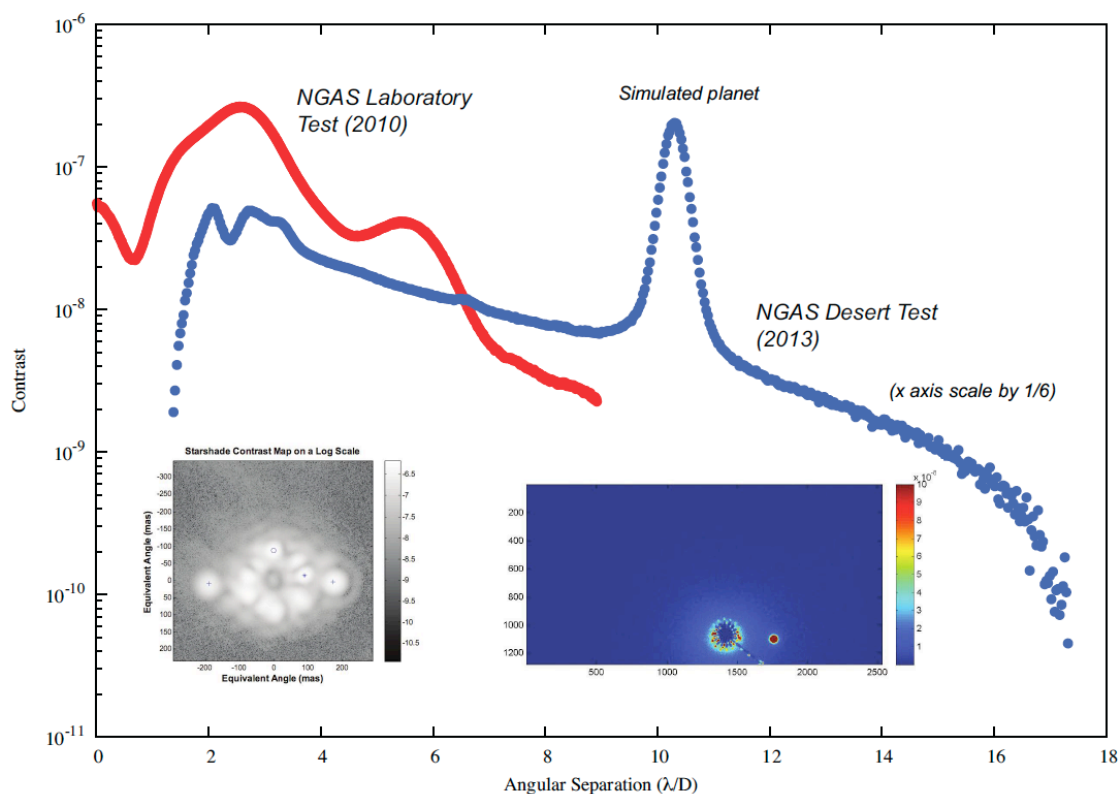


Figure A.3: Starshade demonstrations in the lab and in the desert with 50% bandwidth

## A.4.3   Precision Petal Manufacturing

An initial challenge of constructing a starshade is to demonstrate that the mechanical tolerances for a petal can be met, as derived from a complete starshade error budget. Prior work at NGAS demonstrated that precision petal tips and valleys are manufacturable to the required tolerances [69]. Work underway at Princeton University in 2012 has been directed toward the demonstration of a continuous petal edge, with a Milestone phrased as follows:

On a single full-scale petal made of flight-like materials, measure the edge position relative to a fiducial origin at a sufficient number of locations along the edge. Using optical modeling tools, verify that the predicted mean contrast in the image plane from a uniform field propagated past an occulter with petals of the measured shape in an annulus of width equal to the full-width half-max of the telescope point spread function at the smallest inner working angle is $3 \times 10^{-10}$ or better, the allocated contrast to static errors. Repeat the measurements and analysis a sufficient number of times to give 95% confidence that the predicted contrast is correct [70] [71].

A Milestone in precision petal manufacturing is to demonstrate that a single petal can be manufactured to the design tolerances. This may include a demonstration of the manufacturing of petal edges, tips, and valleys. A representative set of manufacturing tolerances would be demonstrated that derive from error budget allocations.

This work was conducted by N. J. Kasdin (Princeton University) and collaborators through a 2009 TDEM award and successfully completed in 2012 [71].

## A.4.4   Starshade Petal Deployment

After the static mechanical tolerances are demonstrated, a subsequent challenge is to demonstrate that the deployment tolerances for a petal can be met, as derived from a complete starshade error budget.

A Milestone for starshade deployment is to demonstrate that an external occulter can be deployed repeatedly to within the budgeted tolerances. This may be accomplished using single or multiple petals whose manufacturing tolerances have been demonstrated previously.

N. J. Kasdin (Princeton University) and collaborators were funded through a 2010 SAT-TDEM award to demonstrate starshade deployment. The goal was to demonstrate that fiducials at the base of starshade petals could be deployed with radial and lateral position errors less than 1 mm (3-$\sigma$) with 90% confidence. Preliminary results have shown deployments with position repeatability better than 125 $\mu$m (3-$\sigma$).

## A.4.5   Petal Prototype Demonstration

An additional step in the technology maturation of a starshade petal is to integrate in a single demonstration 1) the manufacturing of the required profile, technologies for the control of scattered sunlight (sunlight baffles, sub-micron edges); 2) the multi-layer blankets that cover the opaque regions of the starshade; 3) packaging restraints, and 4) deployment mechanisms.

A Milestone for a petal prototype demonstration would be to demonstrate through hardware and modeling that all the static and dynamic error budget allocations will be met with a design-specific high-fidelity petal.

## A.4.6   Formation Flying Sensors

The starshade and telescope must move one with respect to the other between targets and maintain alignment during science observations. The required technology may include beacons and sensors to detect relative position, and algorithms for high-precision alignment.

A Milestone in formation flying guidance, navigation and control would be to demonstrate that the GN&C algorithms and sensors of an external occulter can achieve the budgeted alignment tolerances. This may include hardware and/or software simulations that demonstrate traceability to flight conditions.

# A.5 Conclusion

The 2010 Astrophysics Decadal Survey recommended the creation of a technology development program for a potential future exoplanet mission to mature starlight-suppression technology for the detection of spectra of Earth-like exoplanets. The Exoplanet Exploration Program supports a community-based process to help NASA select a single architecture by about 2015, and to mature the selected concept for recommendation in the 2020 Decadal Survey. This appendix outlines technology development that will lead toward that goal.

A new appendix will be released each year to update the progress made in each technology area and to identify new SAT-TDEM selections.

# A.6 Bibliography

[1]    NRC Astronomy and Astrophysics Survey Committee, New Worlds, New Horizons in Astronomy and Astrophysics, The National Academies Press, Washington, DC, 2010.

[2]    Traub, W. A., & Oppenheimer, B. R. 2010, "Direct Imaging of Exoplanets," in *Exoplanets*, Seager, S., ed., University of Arizona Press, pp. 111–156.

[3]    Mawet, D., Pueyo, L., Lawson, P., et al. 2012, "Review of small-angle coronagraphic techniques in the wake of ground-based second-generation adaptive optics systems," Proc. SPIE 8442, 844204.

[4]    Lawson, P. R., Belikov, R., Cash, W., et al. 2013, "Survey of experimental results in high-contrast imaging for future exoplanet missions," Proc. SPIE 8864, 88641F.

[5]    Trauger, J. T., & Traub, W. A. 2007, "A laboratory demonstration of the capability to image an Earth-like extrasolar planet," Nature 446, pp. 771–773.

[6]    Mawet, D., Serabyn, E., Liewer, K., et al. 2009, "Optical Vectorial Vortex Coronagraphs using Liquid Crystal Polymers: theory, manufacturing and laboratory demonstration," Optics Express 17, pp. 1902–1918.

[7]    Guyon, O. 2003, "Phase-induced amplitude apodization of telescope pupils for extrasolar terrestrial planet imaging," Astron. Astrophys. 404, pp. 379–387.

[8]    Kasdin, N. J., Carlotti, A., Pueyo, L., Groff, T., Vanderbei, R. 2011, "Unified coronagraph and wavefront control design," Proc. SPIE 8151, 81510Y

[9]    Lyon, R. G., Clampin, M., Woodruff, R. A., et al. 2010, "Visible nulling coronagraphy testbed development for exoplanet detection," Proc. SPIE 7731.

[10]  Moody, D. C., Gordon, B. L., & Trauger, J. T. 2008, "Design and demonstration of hybrid Lyot coronagraph masks for improved spectral bandwidth and throughput," Proc. SPIE 7010.

[11]  Trauger, J., Moody, D., Gordon, B., Krist, J., Mawet, D. 2011, "A hybrid Lyot Coronagraph for the direct imaging and spectroscopy of exoplanet systems," Proc. SPIE 8151, 81510G.

[12]  Kern, B., Kuhnert, A., & Trauger, J.  2008, eds., Exoplanet Exploration Technology Milestone #2 Report, Jet Propulsion Laboratory Publications, Pasadena, California, JPL Document 60951.

[13]  Trauger, J., Stapelfeldt, K., Traub, W., et al. 2010, "ACCESS: a concept study for the direct imaging and spectroscopy of exoplanetary systems," Proc. SPIE 7731, pp. 773128–+.

[14]  Trauger, T., Kern, B., & Kuhnert A., eds., 2006, TPF-C Technology Milestone #1 Report, Jet Propulsion Laboratory Publications, Pasadena, California, JPL Document 35484.

[15]  Shaklan, S., 2009, Exoplanet Exploration Coronagraph Technology Milestone #3A White Paper: Coronagraph Stalight Suppression Model Validation, Jet Propulsion Laboratory Publications, Pasadena, California, JPL Document 64582.

[16]  Soummer, R., Pueyo, L., Ferrari, A., et al. 2009, "Apodized pupil Lyot coronagraphs for arbitrary apertures. II. Theoretical properties and application to extremely large telescopes," Astrophys. J. 695, 695-706.

[17]  Mawet, D., Serabyn, E., Wallace, J. K., & Pueyo, L. 2011, "Improved high-contrast imaging with on-axis telescopes using a multistage vortex coronagraph," Opt. Lett. 36, 1506-1508.

[18]  Guyon, O., Kern, B., Belikov, R., et al. 2012, "Phase Induced Amplitude Apodization (PIAA) coronagraphy: Recent results and future prospects," Proc. SPIE 8442, 84424V.

[19]  Carlotti, A., Kasdin, N. J., Vanderbei, R. J., Delorme, J.-R. 2012, "Optimized shaped pupil masks for pupil with obscuration," Proc. SPIE 8442, 844254.

[20]  Riggs, A. J. E., Groff, T. D., Carlotti, A., et al. 2013, "Demonstration of symmetric dark holes using two deformable mirrors at the high-contrast imaging testbed," Proc. SPIE 8864, 88640T.

[21]  Trauger, J., Gordon, B., Krist, J. et al. 2010, "Technology Milestone Whitepaper: Hybrid Lyot Coronagraph Technology – Linear Masks," Jet Propulsion Laboratory Doc. D-64843. http://exep.jpl.nasa.gov/technology.

[22]  Trauger, J., Moody, D., Gordon, B., Krist, J., and Mawet, D. 2012, "Complex apodization Lyot coronagraphy for the direct imaging of exoplanet systems: design, fabrication, and laboratory demonstration," Proc. SPIE 8442, 84424Q.

[23]  Belikov, R., Pluzhnik, Witteborn, F. C., et al. 2011, "Laboratory demonstration of high-contrast imaging at inner working angles better than 2 λ/D and better," Proc. SPIE 8151, 815102.

[24]  Kern, B., Guyon, O., Give'on, A., Kuhnert, A., Niessner, A. 2011, "Laboratory testing of a Phase-Induced Amplitude Apodization (PIAA) coronagraph," Proc. SPIE 8151, 815104.

[25] Guyon, O., Schneider, G., Close, L. et al. 2010, "Technology Milestone Whitepaper: Phase-Induced Amplitude Apodization Coronagraph: Monochromatic Contrast Demonstration," Jet Propulsion Laboratory Doc. D-65830. http://exep.jpl.nasa.gov/technology.

[26] Guyon, O., Schneider, G., Close, L., et al. 2011, "Technology Milestone #2 Whitepaper: Instrument Tip-Tilt Control Demonstration at the sub-Milliarcsecond Level," Jet Propulsion Laboratory Doc. D-71066. http://exep.jpl.nasa.gov/technology.

[27] Guyon, O., Kern, B., Belikov, R., et al. 2012, "Phase Induced Amplitude Apodization (PIAA) coronagraphy: Recent results and future prospects," Proc. SPIE 8442, 84424V.

[28] Kern, B. D., Guyon, O., Kuhnert, A., et al. 2013, "Laboratory demonstration of Phase Induced Amplitude Apodization (PIAA) coronagraph with better than $10^{-9}$ contrast," Proc. SPIE 8864, 88640R.

[29] Sidick, E., Kern, B., Kuhnert, A., et al. 2013, "Comparisons of simulated contrast performance of different Phase Induced Amplitude Apodization (PIAA) coronagraph configurations," Proc. SPIE 8864, 88641Y.

[30] Mawet, D. P., Serabyn, E., Moody, D., et al. 2011, "Recent results of the second generation of vector vortex coronagraphs on the High Contrast Imaging Testbed at JPL," Proc. SPIE 8151, 81511D.

[31] Serabyn, E., Mawet, D., Burruss, R. 2010, "An image of an exoplanet separated by two diffraction beamwidths from a star," Nature 464, 1018.

[32] Mawet, D., Serabyn, E., Wallace, J. K., et al. 2011, "Improved high-contrast imaging with on-axis telescopes using a multistage vortex coronagraph," Opt. Lett. 36, 1506.

[33] Serabyn, G., Krist, J., Mawet, D., Moody, D., and Trauger, J. 2012, "Technology Milestone Whitepaper: Vortex Coronagraph Technology," Jet Propulsion Laboratory Doc. D-73329. http://exep.jpl.nasa.gov/technology.

[34] Serabyn, E., Trauger, J. T., Moody, D., et al. 2013, "High-contrast imaging results with the vortex coronagraph," Proc. SPIE 8864, 88640Y.

[35] Stewart, J. B., Bifano, T. G., Cornelissen, S., Bierden, P., Levine, B. M., Cook, T. 2007, "Design and development of a 331-segment tip-tilt-piston mirror array for space-based adaptive optics," Sensors and Actuators A 138, 230-238.

[36] Helmbrecht, M. A., He, M., Kempf, C. J. 2012, "Development of high-order segmented MEMS deformable mirrors," Proc. SPIE 8253, 825307.

[37] Lyon, R. G., Clampin, M., Petrone, P., Mallik, U., Madison, T., and Bolcar, M. R. 2012, "High contrast Vacuum Nuller Testbed (VNT) contrast, performance and null control," Proc. SPIE 8442, 844208.

[38] Lyon, R. G., Clampin, M., Petrone, P., et al. 2011, "Vacuum nuller testbed (VNT) performance, characterization and null control: progress report," Proc. SPIE 8151, 81510G.

[39] Clampin, M. 2011, "Technology Milestone #1 Whitepaper: Visible Nulling Coronagraph Technology Maturation: High Contrast Imaging and Characterization of Exoplanets," Jet Propulsion Laboratory Doc. D-68671. http://exep.jpl.nasa.gov/technology.

[40] Belikov, R., Give'on, A., Kern, B., et al. 2007, "Demonstration of high contrast in 10% broadband light with the shaped pupil coronagraph," Proc. SPIE 6693.

[41] Pueyo, L., Kay, J., Kasdin, N. J., et al. 2009, "Optimal dark hole generation via two deformable mirrors with stroke minimization," Appl. Opt. 48, pp. 6296–6312.

[42] Groff, T. D., Kasdin, N. J., Carlotti, A., and Eldorado Riggs, A. J. 2012, "Broadband focal plane wavefront control of amplitude and phase aberrations," Proc. SPIE 8442, 84420C.

[43] Sidick, E., Shaklan, S., Give'on, A., Kern, B. 2011, "Studies of the effects of optical system errors on the HCIT contrast performance," Proc. SPIE 8151, 815106.

[44] Sidick, E., Shaklan, S., Balasubramanian, K. 2012, "HCIT broadband contrast performance sensitivity studies," Proc. SPIE 8520, 85200M.

[45] Krist, J., Belikov, R., Mawet D. et al. 2012, "Technology Milestone #1 Report: Assessing the performance limits of internal coronagraphs through end-to-end modelling," Jet Propulsion Laboratory Doc. D-74425. http://exep.jpl.nasa.gov/technology.

[46] Krist, J. E., Belikov, R., Pueyo, L., et al. 2011, "Assessing the performance limits of internal coronagraphs through end-to-end modelling: a NASA TDEM study," Proc. SPIE 8151, 81510E.

[47] Krist, J. E., Belikov, R., Pueyo, L., et al. 2011, "Assessing the performance limits of internal coronagraphs through end-to-end modelling," Proc. SPIE 8864, 88640P.

[48] Krist, J., Belikov, R., Mawet D. et al. 2012, "Technology Milestone #2 Report: Assessing the performance limits of internal coronagraphs through end-to-end modelling," Jet Propulsion Laboratory Doc. D-74426. http://exep.jpl.nasa.gov/technology.

[49] Galicher, R., Baudoz, P., Rousset, G., et al. 2010, "Self-coherent camera as a focal plane wavefront sensor: simulations," A&A 509, A.31.

[50] Give'on, A., Shaklan, S., Kern, B., Noecker, C., Kendrick, S., and Wallace, K. 2012, "Electric field reconstruction in the image plane of a high-contrast coronagraph using a set of pinholes around the Lyot plane," Proc. SPIE 8442, 84420B.

[51] Shaklan, S., Kern, B., Give'on, A., et al. 2012, "Technology Milestone Report: Advancing Speckle Sensing for Internal Coronagraphs," Jet Propulsion Laboratory Document D-73509. http://exep.jpl.nasa.gov/technology.

[52] Enya, K., Abe, L., Takeuchi, S., et al., 2011, "A high dynamic-range instrument for SPICA for coronagraphic observation of exoplanets and monitoring of transiting exoplanets," Proc. SPIE 8146, 81460Q.

[53] Mendillo, C. B., Hicks, B. A., Cook, T. A., et al. 2012, "PICTURE: a sounding rocket experiment for direct imaging of an extrasolar planetary environment," Proc. SPIE 8442, 84420E.

[54] Turnbull, M. C., Glassman, T., Roberge, A., et al. 2012, "The search for habitable worlds. 1: The viability of a starshade mission," Pub. Astron. Soc. Pac. 124, 418-447.

[55] Shaklan, S. B., Noecker, M. C., Glassman, T., et al. 2010, "Error budgeting and tolerancing of starshades for exoplanet detection," Proc. SPIE 7731, 77312G.

[56] Shaklan, S. B., Marchen, L., Lisman, P. D., et al. 2011, "A starshade petal error budget for exo-earth detection and characterization," Proc. SPIE 8151, 815113.

[57] Copi, C. J., and Starkman, G. D. 2000, "The Big Occulting Steerable Satellite (BOSS)," Astrophys. J. 532, 581–592.

[58] Cash, W. 2006, "Detection of Earth-like planets around nearby stars using a petal-shaped occulter," Nature 442, pp. 51–53.

[59] Vanderbei, R. J., Cady, E., & Kasdin, N. J. 2007, "Optimal Occulter Design for Finding Extrasolar Planets," Astrophys. J. 665, pp. 794–798.

[60] Cady, E. 2011, "Nondimensional representations for occulter design and performance evaluation," Proc. SPIE 8151, 815112.

[61] Lo, A., Cash, W., Hyde, T., Polidan, R., & Glassman, T. 2009, "Starshade Technology Development: Astro2010 Technology Development Whitepaper," ArXiv Astrophysics e-prints 2010, pp. 44–+.

[62] Cash, W., Kendrick, S., Noecker, et al., 2009, "The New Worlds Observer: the astrophysics strategic mission concept study," Proc. SPIE 7436.

[63] Thomson, M. W., Lisman, P. D., Helms, R., et al. 2010, "Starshade design for occulter based exoplanet missions," SPIE 7731.

[64] Kasdin, N. J., Spergel, D. N., Lisman, D., et al. 2011, "Advancing technology for starlight suppression via an external occulter," Proc. SPIE 8151, 81510J.

[65] Kasdin, N. J., Lisman, D., Shaklan, S., et al. 2013, "Verifying occulter deployment tolerances as part of NASA's technology development for exoplanet missions," Proc. SPIE 8864, 886417.

[66] Sirbu, D., Cady, E., Kasdin, N. J., et al. 2011, "Optical verification of occulter-based high contrast imaging," Proc. SPIE 8151, 815114.

[67] Sirbu, D., Kasdin, N. J., Vanderbei, R. J., 2013, "Progress on optical verification for occulter-based high contrast imaging," Proc. SPIE 8864, 886419.

[68] Samuele, R., Varshneya, R., Johnson, T. P., et al. 2010, "Progress at the starshade testbed at Northrop Grumman Aerospace Systems: comparisons with computer simulations," Proc. SPIE 7731.

[69] Lo, A. S., Glassman, T., Dailey, D., Sterk, K., Green, J., Cash, W., Soummer, R. 2010, "New Worlds Probe," Proc. SPIE 7731, 77312E.

[70] Kasdin, N. J., Lisman, D., Shaklan, S., et al. 2012, "Technology demonstration of starshade manufacturing for NASA's Exoplanet Mission Program," Proc. SPIE 8442, 84420A.

[71] Kasdin, N. J., Spergel, D. N., Vaderbei, R., et al. 2012, "Technology Milestone Report: Advancing Technology for Starlight Suppression via an External Occulter," Jet Propulsion Laboratory Document D-74384. http://exep.jpl.nasa.gov/technology.

[72] Martin, S. R., Shaklan, S. B., Crawford, S. L., et al. 2013, "Starshade optical edge modelling, requirements, and laboratory tests," Proc. SPIE 8864, 88641A.

[73] Glassman, T., Casement, S., Warwick, S., et al. 2013, "Achieving high-contrast ratios with a 60-cm starshade," Proc. SPIE 8864, 886418.

[74] Figer, D. 2010, "Technology Milestone Whitepaper: A Photon-Counting Detector for Exoplanet Missions," Jet Propulsion Laboratory Doc. D-66493. http://exep.jpl.nasa.gov/technology.

[75] Figer, D., Lee, J., Hanold, B. J., et al. 2011, "A photon-counting detector for exoplanet missions," Proc. SPIE 8151, 81510K.